ELSEVIER

Polymer 41 (2000) 4651–4659

polymer

The semicrystalline morphology of aliphatic–aromatic polyamide blends

C.S. Powell[a], D.S. Kalika[a,b,*]

[a]*Department of Chemical and Materials Engineering, University of Kentucky, Lexington, KY 40506-0046, USA*
[b]*Center for Robotics and Manufacturing Systems, University of Kentucky, Lexington, KY 40506-0046, USA*

Received 30 June 1999; received in revised form 15 September 1999; accepted 17 September 1999

Abstract

The morphology of a series of melt-miscible blends based on the combination of (crystalline) polyamide (PA) 4,6 and (amorphous) PA 6I has been investigated as a function of blend composition and thermal history. Wide-angle X-ray scattering (WAXS) was used to determine the unit cell structure and crystallinity index in PA 4,6 and the blends: the introduction of PA 6I resulted in no change in unit cell parameters and a monotonic decrease in bulk crystallinity. Dynamic mechanical studies revealed the coexistence of two amorphous phases in the crystallized blends: a mixed phase held between the crystal lamellae (interlamellar) and a PA 6I-rich phase excluded to interfibrillar and interspherulitic regions. There was no evidence of a separate crystal–amorphous interphase layer comprised of pure PA 4,6. Transamidation reactions over longer melt times led to the apparent homogenization of the two amorphous populations owing to the formation of increasingly random copolymers. © 2000 Elsevier Science Ltd. All rights reserved.

Keywords: Polyamides; Crystallizable blends; Transamidation

1. Introduction

The morphology of binary polymer blends containing a single crystallizable component has been the subject of considerable investigation over the past decade. Of particular interest has been the evolution of semicrystalline morphology in melt-miscible blends as influenced by the characteristics of the constituents and the thermal history of the blend. One basis by which to describe the morphology that is encountered in these blends concerns the disposition of the non-crystallizable diluent in the semicrystalline microstructure. As crystallization proceeds, the diluent is excluded from the evolving crystals, with the melt correspondingly enriched in this non-crystallizable component. Ultimately, the amorphous diluent may reside in *interlamellar*, *interfibrillar*, or *interspherulitic* regions, or some combination thereof. The morphology that results in the crystallized blend reflects the nature and extent of interaction between the blend components, the mobility of the diluent, and the crystal growth rate.

The morphology observed in melt-miscible polymer blends depends upon the ability of the crystallizable polymer to accommodate non-crystallizable diluent between the crystal lamellae. For blends based on relatively flexible crystalline polymers, a large degree of interlamellar accommodation is typically encountered. This is the case for blends of poly(vinylidene fluoride) with poly(methyl methacrylate) [1–5], as well as poly(ethylene oxide) with poly(methyl methacrylate) [6,7]. Dielectric relaxation studies on these blends reveal the coexistence of two amorphous phases: a homogeneous mixed phase located at the center of the amorphous interlayer, and a distinct crystal–amorphous "interphase" region comprised of pure crystallizable polymer. This interphase layer is necessitated by the difficulty in dissipating order at the crystal surface, and results in demixing of the crystallizable and non-crystallizable components over a distance of ~1.5–3 nm as predicted by lattice calculations [8,9] (see discussion of crystal–amorphous interphases in Ref. [10]). For blends based on less flexible polymers (e.g. poly(butylene terephthalate) with bisphenol A polyarylate [11–15]; poly(ether ether ketone) with poly(etherimide) [16–21]), only a limited amount of interlamellar incorporation of the non-crystallizable diluent is observed. In these blends, a mixed interlamellar amorphous phase coexists with an excluded phase comprised of pure polymeric diluent. A separate crystal–amorphous interphase relaxation is not detected. Kumar and Yoon have attributed the failure to detect a separate crystal–amorphous interphase in these systems to

* Corresponding author. Department of Chemical and Materials Engineering, 177 Anderson Hall, University of Kentucky, Lexington, KY 40506-0046, USA. Tel.: +1-606-257-8572; fax: +1-606-323-1929.
E-mail address: kalika@engr.uky.edu (D.S. Kalika).

0032-3861/00/$ - see front matter © 2000 Elsevier Science Ltd. All rights reserved.
PII: S0032-3861(99)00695-3

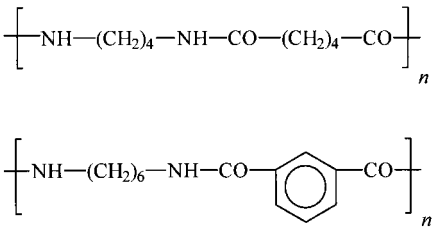

Fig. 1. Repeat unit structures for PA 4,6 and PA 6I.

the penetration of the interphase region by the non-crystallizable chains, leading to a mixed layer that is indistinguishable from the bulk interlamellar material [9].

While the inherent structural characteristics of the blend constituents have a strong influence on the morphology that is observed, kinetic factors are also important, specifically the rate at which the diluent can diffuse away from the evolving crystals as compared to the rate of crystal growth. The length scale of diluent segregation reflects the relative magnitude of these factors [22,23]: under conditions where the rate of crystallization is fast as compared to the rate of diluent diffusion, interlamellar trapping is favored, while under conditions where the rate of crystallization is slow as compared to diluent diffusion, interfibrillar or interspherulitic morphologies are obtained. This was explored systematically by Talibuddin et al. [24], who performed small-angle X-ray scattering (SAXS) studies on a series of model blends based on PEO in which the non-crystallizable diluent was varied in order to assess the importance of diluent mobility and polymer–polymer interaction on morphology. For blend pairs in which polymer–polymer interactions were weak, the resulting microstructure correlated with diluent mobility; the high-T_g (low mobility) diluent was found to reside exclusively between the crystal lamellae, while the low-T_g (high mobility) diluent was partially excluded to interfibrillar regions. However, when strongly interacting blend pairs were examined, diluent mobility was not a factor. The presence of strong interactions between the blend components led to a significant reduction in overall crystal growth rate and a correspondingly larger segregation length scale, independent of diluent mobility. For a comprehensive discussion of the various microstructures observed in crystallizable polymer blends, see Debier et al. [25].

In this paper, the morphological characteristics of a series of blends based on polyamide (PA) 4,6 and PA 6I have been investigated by X-ray scattering and dynamic thermal analysis methods. PA 4,6 is an aliphatic polyamide that crystallizes rapidly from the melt, while PA 6I is an aromatic polyamide that remains fully amorphous in the solid state owing to the presence of a 1,3-connected phenylene (i.e. isophthalate) linkage in the repeat (see Fig. 1). The DSC glass transition temperatures for PA 4,6 and PA 6I are 75 and 130°C, respectively [26]. The miscibility characteristics of a wide spectrum of aliphatic–aromatic PA blend pairs have been assessed by Ellis [27,28], who elucidated the structural and chemical features governing the phase behavior of these systems. Ellis reported that PA 4,6 is fully miscible with PA 6I in all proportions.

An important consideration in characterizing the morphology of these PA blends is their ability to undergo transamidation reactions in the melt state leading to the formation of copolymers. Groeninckx and co-workers have reported detailed ^{13}C NMR and calorimetric studies in which the transreaction of the PA 4,6/PA 6I blends was correlated with the crystallization behavior and the resulting microstructure [26,29–32]. Even at relatively short melt times, transamidation led to a marked decrease in the rate of crystallization owing to the incorporation of PA 6I segments into the otherwise highly regular PA 4,6 chains. At longer melt times, increasingly random copolymers were obtained. However, even at the longest melt times and highest temperatures examined, the chains retained a certain degree of blockiness, such that crystallization was still possible (blends containing >30% PA 4,6). In the studies reported here, all blends were formulated from solution in order to avoid transamidation reactions prior to the imposition of a well-defined thermal history.

2. Materials and experimental methods

Commercial grade PA 4,6 (Stanyl TW341) was obtained in pellet form through the courtesy of DSM Engineering Plastics. PA 6I (Durethan T40) pellets were obtained through the courtesy of Bayer Polymers Division. Blends were prepared by dissolution of the resin pellets in 90% formic acid (1–2 wt% polymer) followed by precipitation with excess deionized water. The filtered precipitate was washed with hot water and dried under vacuum (80°C; 0.1 Torr) for a minimum of 48 h prior to film fabrication.

Sample films (0.20 mm thickness) were prepared by compression molding the blend powder in a Carver melt press at 305°C. Hold time in the melt ranged from 2 to 10 min. The films were isothermally crystallized by rapid transfer to a second press held at 250°C; the crystallization hold time was 20 min. Full crystallization of all blend compositions over the hold period was verified by independent calorimetric measurements. The films were subsequently stored under vacuum at 80°C.

Wide-angle X-ray scattering (WAXS) was used to assess the index of crystallinity in all blend samples. Sample films were examined in reflection using a Rigaku X-ray diffractometer with CuK_α radiation at room temperature across a range of scattering angles (2θ) from 10 to 45°. For each specimen, the diffraction pattern from an (amorphous) PA 6I film was scaled and subtracted from the semicrystalline result; it was assumed that the scattering of the amorphous segments in the semicrystalline specimens could be reasonably represented by the scattering halo of the wholly amorphous PA 6I. The index of crystallinity was estimated

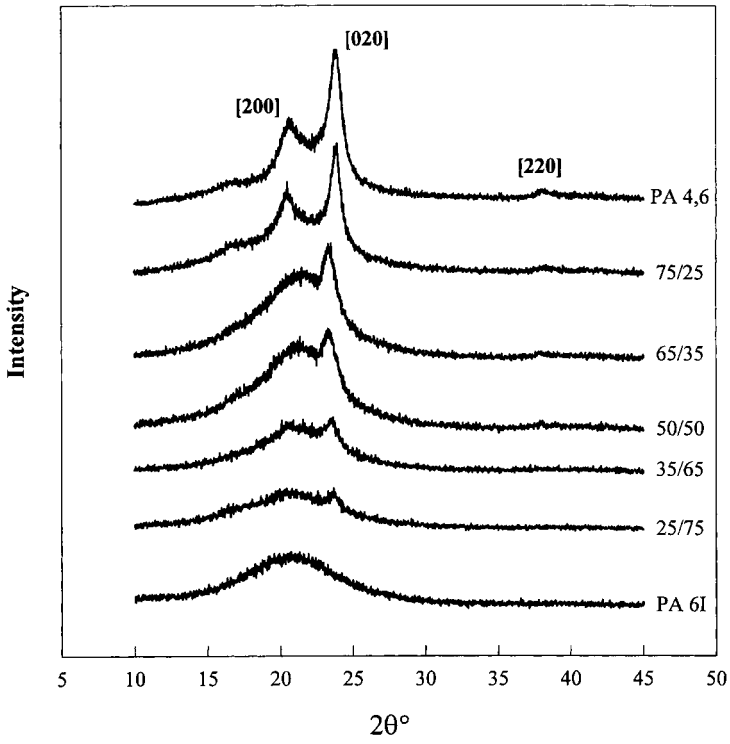

Fig. 2. Wide-angle X-ray diffraction patterns (intensity vs. 2θ) for PA 4,6; PA 6I; and PA 4,6/PA 6I blends. Specimens prepared at 305°C (2 min), with isothermal crystallization at 250°C (20 min).

as the ratio of the net crystalline scattering intensity to the overall scattering intensity.

Calorimetric measurements were performed using the Perkin–Elmer DSC-7 differential scanning calorimeter. Transition temperatures and melting enthalpy were calibrated using indium and zinc standards. All scans were performed under an inert (N_2) atmosphere at a scanning rate of 20°C min^{-1}.

Dynamic mechanical thermal analysis was performed in the vicinity of the glass transition using a Polymer Laboratories DMTA Mk II operating in single cantilever bending geometry. Storage modulus (E') and loss tangent (tan δ) were recorded at a heating rate of 1°C min^{-1} with test frequencies in the range of 0.1–10 Hz. The measurements were carried out under dry (N_2) atmosphere in order to eliminate the influence of moisture on the relaxation characteristics of the PA blends.

Dielectric spectroscopy measurements were accomplished using a Polymer Laboratories dielectric thermal analyzer (PL-DETA) comprised of a GenRad Digibridge interfaced with the Polymer Laboratories temperature controller. Concentric silver electrodes (33 mm) were vacuum evaporated directly on the samples, which were mounted between polished platens in the temperature-controlled test oven; all measurements were carried out under an inert (N_2) atmosphere. The dielectric constant (ε') and loss factor (tan δ) were recorded at frequencies ranging from 0.05 to 100 kHz across a temperature range from 50 to 200°C. The heating rate was 1°C min^{-1}.

3. Results and discussion

WAXS results (intensity vs. 2θ) for PA 4,6 and the blends are reported in Fig. 2. All specimens were prepared at 305°C (2 min), with isothermal crystallization at 250°C (20 min). The three prominent reflections in PA 4,6 located at 20.3, 24.0 and 38.1° (2θ) have been indexed based on a monoclinic unit cell and are consistent with the cell parameters reported by Atkins et al.: the unit cell contains four chain segments, with $a = 0.96$, $b = 0.83$, c (chain axis) = 1.47 nm, and $\gamma = 115°$ [33]. The positions of these reflections are essentially unchanged in the blends as compared to pure PA 4,6, which indicates that the PA 6I segments are not incorporated into the PA 4,6 crystals and do not change the PA 4,6 unit cell. This result is in agreement with time-resolved WAXS studies on PA 4,6 and PA 4,6/PA 6I blends reported by Eersels et al. [32].

The weight fraction crystallinity for the PA 4,6 as determined by WAXS was 0.68. The addition of PA 6I in the blends resulted in a monotonic decrease in the crystalline fraction with increasing PA 6I content (Fig. 3a) which suggests that PA 6I acts as a simple diluent. As such, it was possible to use the wide range of crystallinities encompassed by the blends to predict the heat of fusion for a 100% crystalline specimen. The correlation between crystallinity measured by WAXS and heat of fusion measured by DSC is shown in Fig. 3b; linear extrapolation to 100% crystallinity results in a value for the heat of fusion, $\Delta H_F^0 = 149$ J g^{-1}.

Dynamic mechanical results for the PA 4,6 and PA 6I

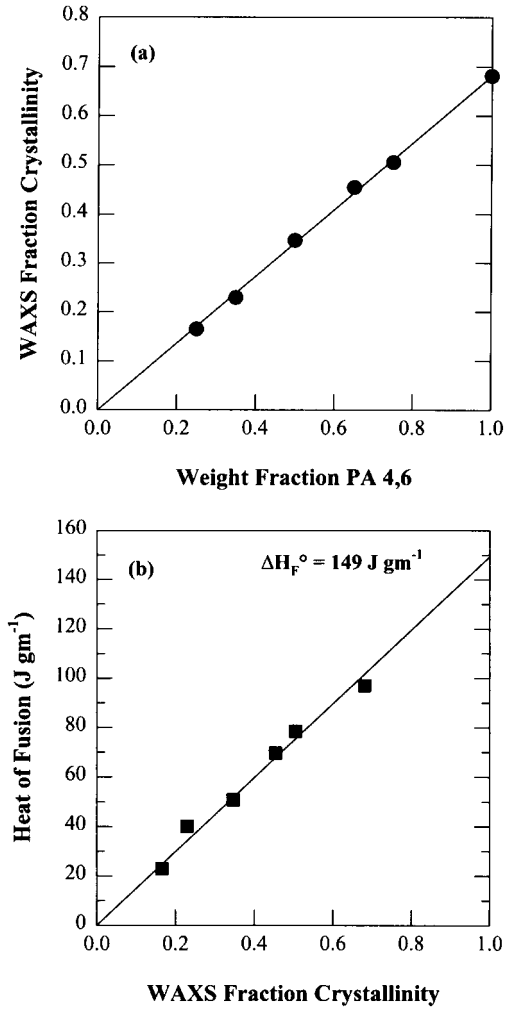

Fig. 3. (a) Weight fraction crystallinity determined by WAXS vs. weight fraction PA 4,6 in the blends; and (b) DSC heat of fusion (J g^{-1}) vs. WAXS fraction crystallinity.

homopolymers are shown in Figs. 4 and 5, respectively. Crystalline PA 4,6 displays a broad maximum in tan δ at the glass transition ($T_{\alpha,0.1\ Hz} = 90°C$). PA 6I displays a sharp, stronger tan δ peak owing to its wholly amorphous character ($T_{\alpha,0.1\ Hz} = 143°C$).

Dielectric sweeps for PA 4,6 and PA 6I are shown in Figs. 6 and 7, respectively. PA 4,6 displays an extremely broad transition that encompasses nearly the entire range of temperature measurement. This transition is comprised of two overlapping polarization events [34]: (i) orientation polarization associated with the mobilization of amorphous chain segments at the glass transition; and (ii) Maxwell–Wagner–Sillars (MWS) interfacial polarization owing to the accumulation of mobile charge carriers at the interfaces between the crystal and amorphous phases [35–37]. Due to the strong overlap between these two polarization events, no attempt was made to separate them by curve-fitting methods. A narrower (glass–rubber) transition is observed for PA 6I; the increase in dielectric constant observed above the glass transition is the result of electrode polarization.

Dynamic mechanical thermal analysis and dielectric relaxation spectroscopy are powerful tools for the elucidation of phase behavior in crystalline polymer blends. Both methods provide high sensitivity for the detection of motional transitions (e.g. the glass transition), and can be used to determine the number and composition of the individual amorphous phases present in the blend. The usefulness of DMTA or DETA for the detection of multiple amorphous phases depends upon the relative glass–rubber relaxation timescales of the individual constituents. If the relaxation timescales of the blend components are markedly different (T_g's separated by 20–30°C, or more), then the presence of multiple amorphous phases of differing composition will be detectable as separate relaxation events in a dynamic mechanical or dielectric experiment. If, however, the relaxation timescales/relaxation temperatures of the

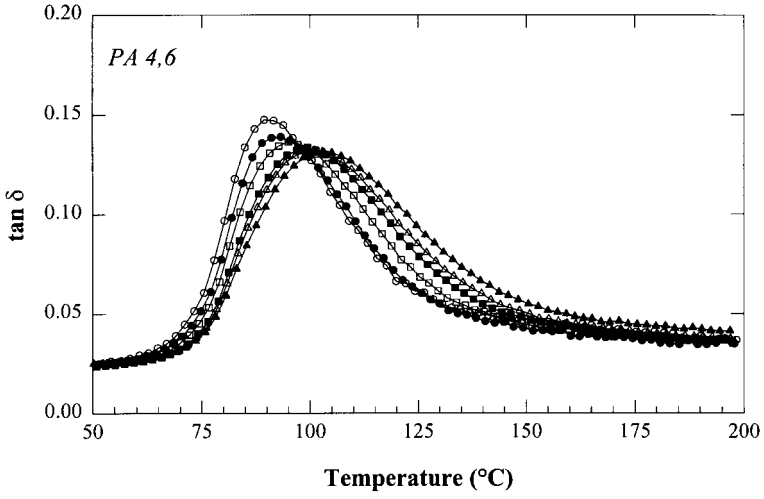

Fig. 4. Dynamic mechanical tan δ vs. temperature (°C) for PA 4,6 isothermally crystallized at 250°C. Frequencies of 0.1, 0.3, 1, 3, 5, 10 Hz.

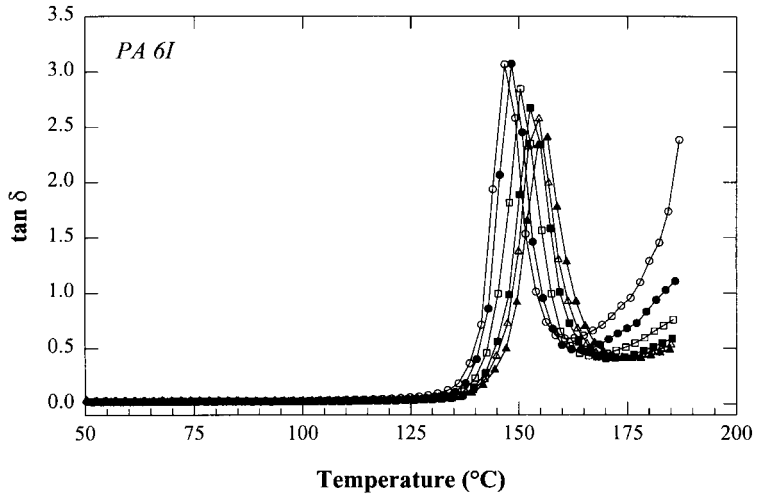

Fig. 5. Dynamic mechanical tan δ vs. temperature (°C) for PA 6I. Frequencies of 0.1, 0.3, 1, 3, 5, 10 Hz.

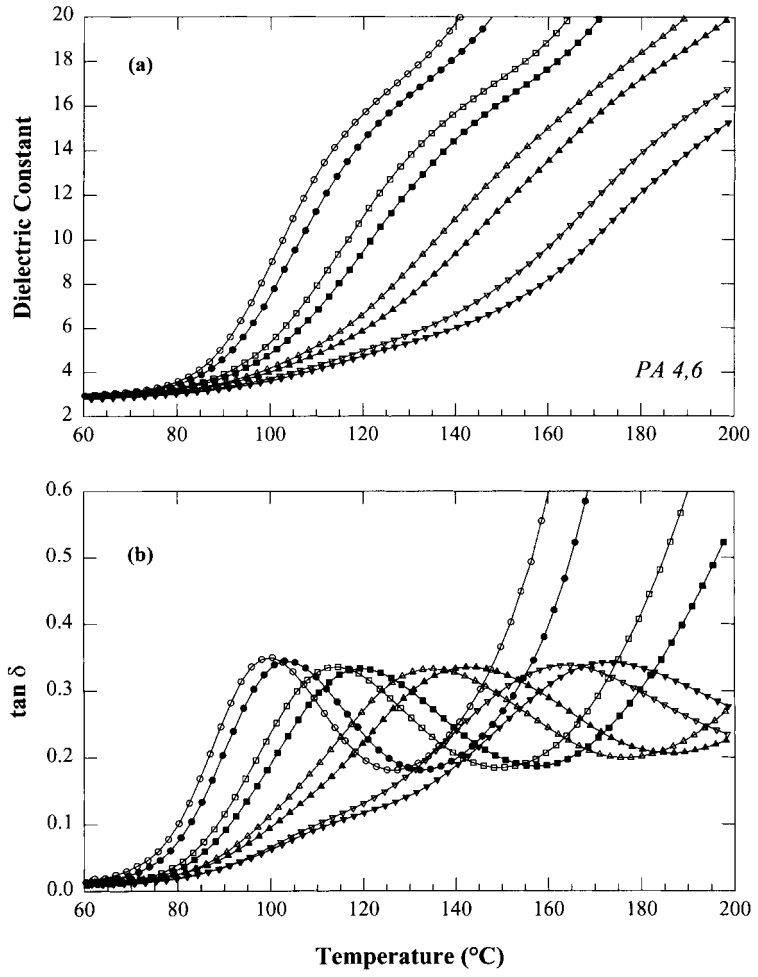

Fig. 6. Dielectric constant and tan δ vs. temperature (°C) for PA 4,6 isothermally crystallized at 250°C. Frequencies of 0.05, 0.1, 0.5, 1, 5, 10, 50, 100 kHz.

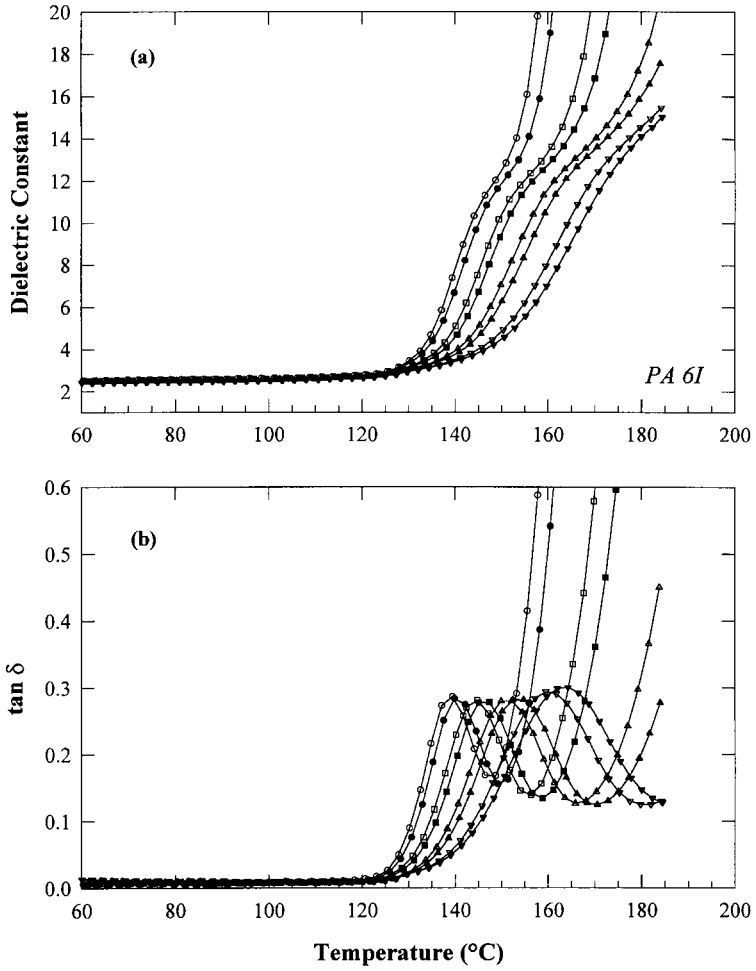

Fig. 7. Dielectric constant and tan δ vs. temperature (°C) for PA 6I. Frequencies of 0.05, 0.1, 0.5, 1, 5, 10, 50, 100 kHz.

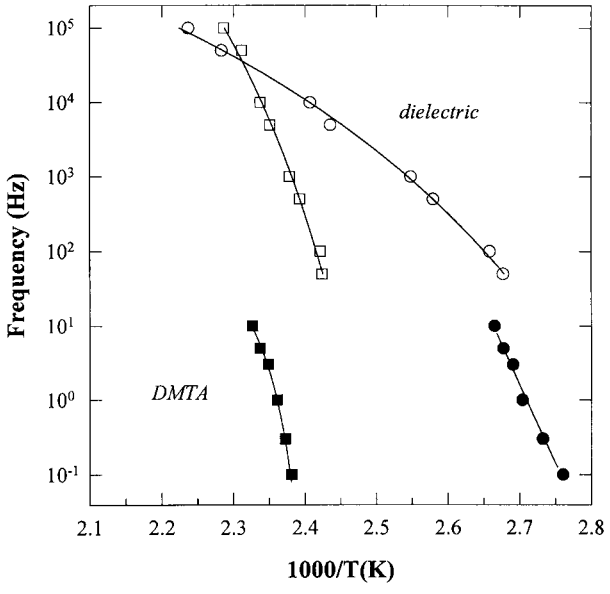

Fig. 8. Arrhenius plot of test frequency (Hz) vs. $1000/T_{MAX}$ based on isochronal temperature sweeps. ○, PA 4,6; □, PA 6I. Open symbols correspond to dielectric results; filled symbols correspond to dynamic mechanical results.

constituents are similar, only a single, broad relaxation is likely to be detected regardless of the phase state of the material.

The viability of the dynamic mechanical and dielectric methods for discerning multiple amorphous phases in the PA blends was assessed via construction of an Arrhenius plot of frequency vs. $1000/T_{MAX}$ for PA 4,6 and PA 6I (Fig. 8). In the dynamic mechanical experiments, PA 4,6 and PA 6I display comparable apparent activation energies, with a separation in T_α between the two polymers of ~50°C across the entire frequency range of measurement. In the dielectric studies, however, PA 4,6 displays a much lower apparent activation energy as compared to PA 6I, and as a result the two relaxations overlap at higher frequencies. This behavior reflects the strong influence that MWS polarization has on the measured dielectric relaxation characteristics of PA 4,6. DMTA is clearly better suited for the elucidation of amorphous phase behavior in the PA 4,6/PA 6I blends owing to the large separation in constituent relaxation temperatures that is obtained in the dynamic mechanical measurements, and the absence of dielectric conduction processes that can obscure the glass transition event.

Dynamic mechanical results for the PA 4,6/PA 6I blend

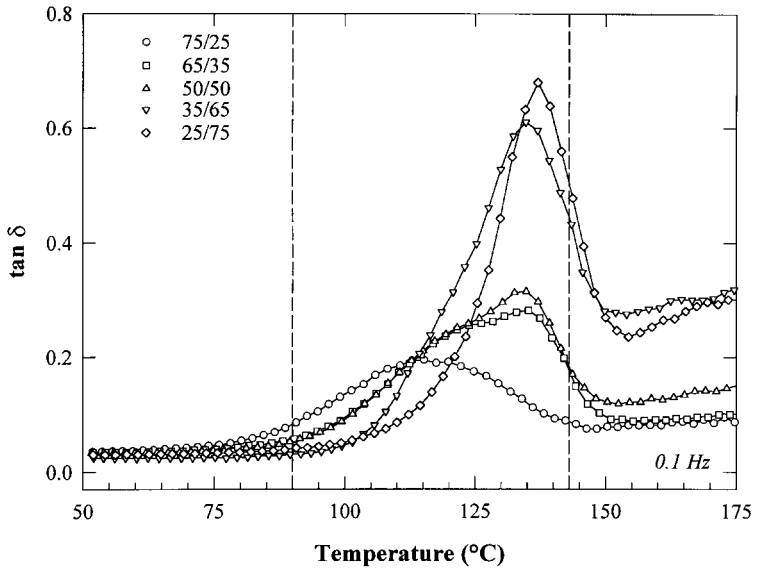

Fig. 9. Dynamic mechanical tan δ vs. temperature (°C) for PA 4,6/PA 6I blends (0.1 Hz). All specimens prepared at 305°C (2 min), with isothermal crystallization at 250°C (20 min). Vertical lines indicate dynamic mechanical peak temperatures for PA 4,6; PA 6I, respectively.

compositions are plotted as tan δ vs. temperature (0.1 Hz) in Fig. 9; the relaxation temperatures for pure PA 4,6 and PA 6I are indicated as vertical dashed lines on the plot. For the intermediate blend compositions (65/35, 50/50, 35/65 PA 4,6/PA 6I), two relaxation events are evident with increasing temperature corresponding to two distinct amorphous phases. The lower-temperature relaxation is located intermediate to the two pure polymer relaxations and corresponds to a mixed amorphous phase. Application of a simple mixing rule such as the Fox equation [38] indicates a mixed phase composition of 34% PA 4,6 and 66% PA 6I (50/50 blend). The position of the higher-temperature relaxation is essentially independent of composition, and corresponds to a PA 6I-rich phase comprised of 10% PA 4,6 and 90% PA 6I; the intensity of the relaxation increases strongly with PA 6I content in the blend. Based on the known weight fraction crystallinity, the overall phase breakdown for the 50/50 blend is calculated as 34% crystalline PA 4,6; 39% mixed amorphous phase; 27% PA 6I-rich phase.

The isochronal DMTA curves measured for the PA blends are similar in character to dynamic mechanical and dielectric data reported for PBT/PAr [12,15] and PEEK/PEI [20,21]. In the case of both PBT/PAr and PEEK/PEI, a

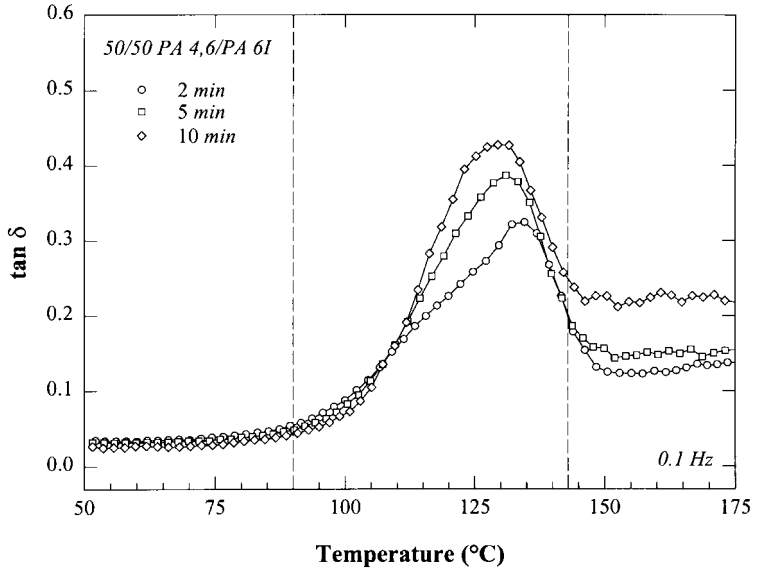

Fig. 10. Dynamic mechanical tan δ vs. temperature (°C) for 50/50 PA 4,6/PA 6I blend (0.1 Hz). Specimens prepared at 305°C for 2, 5, 10 min, respectively, with isothermal crystallization at 250°C (20 min).

strong, higher-temperature relaxation is observed close to the T_g of the non-crystallizable component. This higher-temperature relaxation, which scales in intensity with increasing diluent content, reflects the presence of an extralamellar (i.e. interfibrillar or interspherulitic) pure diluent phase with a sizescale on the order of microns. An accompanying lower-temperature relaxation indicates the coexistence of a mixed interlamellar phase with a sizescale of the order 10 nm. SAXS studies on PBT/PAr and PEEK/PEI support these phase assignments: both blend pairs display a modest amount of interlamellar incorporation at lower overall diluent content, with increasing exclusion to interfibrillar/interspherulitic regions at higher diluent content [15,21]. The results for the PA blends reported here are consistent with the morphologies observed for PBT/PAr and PEEK/PEI, and suggest the coexistence of an interlamellar mixed phase and an excluded phase comprised of nearly pure PA 6I. No PA 4,6 crystal–amorphous interphase is evident from the DMTA measurements. A definitive phase assignment for the observed amorphous phase transitions requires supporting SAXS measurements; these studies will be reported in a subsequent publication [39].

The influence of transamidation on the dynamic mechanical response of the crystallized blends is examined in Fig. 10, wherein tan δ is plotted vs. temperature (0.1 Hz) for a series of 50/50 PA 4,6/PA 6I blend samples that were held in the melt at 305°C for increasing periods of time prior to isothermal crystallization at 250°C. For those samples exposed to longer melt times (and higher extents of transamidation), there is a progressive increase in relaxation intensity and a transformation from two distinct, overlapping relaxations to a single, broad relaxation positioned intermediate to the two original relaxation events. This progression reflects a modest loss of crystallinity in the samples, but also an apparent homogenization of the amorphous phase material at higher degrees of transreaction. Eersels et al. [32] have reported SAXS data for PA 4,6/PA 6I blends melt extruded at 315°C, with subsequent injection molding. For their transreacted samples, a high degree of interlamellar incorporation of the PA 6I was evident, as indicated by a systematic increase in SAXS long period with increasing PA 6I content in the blend. This suggests that as transreaction proceeds, a progressively larger fraction of the non-crystallizable PA 6I is covalently tied to the crystalline PA 4,6 chains, and is thus unable to escape to interfibrillar and interspherulitic regions. As a result, only a single broad glass transition is observed, reflecting the relaxation of a mixed amorphous phase held between the crystal lamellae.

4. Conclusions

The morphology of a series of crystallizable PA blends based on PA 4,6 and PA 6I has been investigated as a function blend composition and thermal history. Combined WAXS and DSC studies showed that PA 6I acts as a simple diluent in the blends, and does not appear to influence the unit cell structure or the degree of crystallinity of PA 4,6 in isothermally crystallized specimens. Dynamic mechanical studies indicated the coexistence of two amorphous phases in the untransreacted blends corresponding to a mixed interlamellar phase and a PA 6I-rich phase excluded to interfibrillar and interspherulitic regions. This phase behavior is similar to that observed for other melt-miscible blend combinations based on less flexible polymers, e.g. PBT/PAr and PEEK/PEI. For samples exposed to increasing degrees of transamidation, only a single amorphous phase relaxation was observed, indicating the progressive homogenization of amorphous material in the blends.

Acknowledgements

The authors are pleased to acknowledge the contributions of T. Brock Jordan and Wendell B. Lake as part of their participation in the NSF Research Experience for Undergraduates program at the University of Kentucky.

References

[1] Morra BS, Stein RS. Polym Engng Sci 1984;24:311.
[2] Hahn B, Wendorff J, Yoon DY. Macromolecules 1985;18:718.
[3] Hahn BR, Herman-Schonherr O, Wendorff JW. Polymer 1987;28:201.
[4] Yoon DY, Ando Y, Rozstaczer S, Kumar SK, Alfonso GC. Macromol Chem, Macromol Symp 1991;50:183.
[5] Ando Y, Yoon DY. Polym J 1992;24:1329.
[6] Russell TP, Ito H, Wignall GD. Macromolecules 1988;21:1703.
[7] Runt J, Barron CA, Zhang X, Kumar SK. Macromolecules 1991;24:3466.
[8] Kumar SK, Yoon DY. Macromolecules 1989;22:4098.
[9] Kumar SK, Yoon DY. Macromolecules 1991;24:5414.
[10] Runt JP. Dielectric studies of polymer blends. In: Runt JP, Fitzgerald JJ, editors. Dielectric spectroscopy of polymeric materials, Washington, DC: American Chemical Society, 1997. p. 283.
[11] Runt JP, Miley DM, Zhang X, Gallagher KP, McFeaters K, Fishburn J. Macromolecules 1992;25:1929.
[12] Runt JP, Zhang X, Miley DM, Gallagher KP, Zhang A. Macromolecules 1992;25:3902.
[13] Runt J, Miley DM, Gallagher KP, Zhang X, Barron CA, Kumar SK. Polym Adv Tech 1994;5:333.
[14] Huo PP, Cebe P. Macromolecules 1993;26:3127.
[15] Huo PP, Cebe P, Capel M. Macromolecules 1993;26:4275.
[16] Harris JE, Robeson LM. J Appl Polym Sci 1988;35:1877.
[17] Crevecoeur G, Groeninckx G. Macromolecules 1990;24:1190.
[18] Hudson SD, Davis DD, Lovinger AJ. Macromolecules 1992;25:1759.
[19] Hsiao BS, Sauer BB. J Polym Sci Phys Ed 1993;31:901.
[20] Bristow JF, Kalika DS. Polymer 1997;38:287.
[21] Jonas AM, Ivanov DA, Yoon DY. Macromolecules 1998;31:5352.
[22] Keith HD, Padden FJ. J Appl Phys 1963;34:2409.
[23] Keith HD, Padden FJ. J Appl Phys 1964;35:1270.
[24] Talibuddin S, Wu L, Runt J, Lin JS. Macromolecules 1996;29:7527.
[25] Debier D, Jonas AM, Legras R. J Polym Sci Phys Ed 1998;36:2197.
[26] Eersels KLL, Groeninckx G. Polymer 1996;37:983.
[27] Ellis TS. Macromolecules 1991;24:3845.
[28] Ellis TS. Macromolecules 1996;29:1836.

[29] Aerdts AM, Eersels KLL, Groeninckx G. Macromolecules 1996;29:1041.
[30] Eersels KLL, Aerdts AM, Groeninckx G. Macromolecules 1996;29:1046.
[31] Eersels KLL, Groeninckx G. J Appl Polym Sci 1997;63:573.
[32] Eersels KLL, Groeninckx G, Koch MHJ, Reynaers H. Polymer 1998;39:3893.
[33] Atkins EDT, Hill M, Hong SK, Keller A, Organ S. Macromolecules 1992;25:917.
[34] Steeman PAM, Maurer FHJ. Polymer 1992;33:4236.
[35] Maxwell JC. Electricity and magnetism, Oxford: Clarendon Press, 1892.
[36] Wagner KW. Arch Electrotech 1914;2:378.
[37] Sillars RW. J Inst Elect Engng 1937;80:378.
[38] Fox TG. Bull Am Phys Soc 1956;1:123.
[39] Loo L, Lake WB, Kalika DS, Register RA, in preparation.